Chapter 5
Molecular Imaging in Head and Neck Squamous Cell Carcinoma Patients

Sjoukje F. Oosting, Elisabeth G.E. de Vries, and Max J.H. Witjes

Introduction

Molecular imaging allows visualization of tumor biology in vivo [1]. Different processes can be visualized, such as glucose metabolism, proliferation, and hypoxia. But also numerous ligands for receptors and other relevant targets in the tumor microenvironment have been labeled to be used as a tracer for molecular imaging. For positron emission tomography (PET) and single photon emission computerized tomography (SPECT) imaging, ligands are labeled with a radioactive nuclide, while for optical imaging ligands are labeled with a fluorescent dye. Also for magnetic resonance imaging (MRI), computerized tomography (CT), and ultrasound, specific contrast agents are available for molecular imaging [2–4]. Head and neck squamous cell carcinoma (HNSCC) is diagnosed in more than 500,000 patients worldwide per year. Many patients present with locally advanced disease, which has a poor prognosis with around 50 % 5-year survival. Adequate staging and tumor delineation could enhance precision of surgery and radiotherapy, which may lead to a reduction of recurrences. PET imaging has great potential to improve staging, while optical imaging is investigated for its ability to improve tumor delineation. Furthermore, molecular imaging can be used to visualize specific tumor characteristics that can be used for targeted treatment. Therefore, this chapter will focus on PET imaging and optical imaging in HNSCC.

S.F. Oosting, MD, PhD (✉) • E.G.E. de Vries
Department of Medical Oncology, University of Groningen, University Medical Center Groningen, PO Box 30 001, 9700 RB Groningen, The Netherlands
e-mail: s.oosting@umcg.nl

M.J.H. Witjes
Department of Oral and Maxillofacial Surgery, University of Groningen, University Medical Center Groningen, PO Box 30 001, 9700 RB, Groningen, The Netherlands

J.B. Vermorken et al. (eds.), *Critical Issues in Head and Neck Oncology*,
DOI 10.1007/978-3-319-42909-0_5

PET Imaging

Next to a role in diagnosis, staging, and response evaluation when combined with CT or MRI, PET imaging maybe useful for prognostication and radiotherapy treatment planning. Furthermore, PET imaging can be used during drug development by demonstrating the distribution of a drug or treatment target [5]. The role of PET in the management of head and neck cancer patients has been summarized in an excellent review by Cammaroto et al. [6]. Radionuclides that are frequently used for PET imaging in patients are fluor-18 (^{18}F), copper-64 (^{64}Cu), zirconium-89 (^{89}Zr), and iodine-124 (^{124}I), which differ among others in half-life (1.8 h, 12.7 h, 78.4 h, and 100.2 h, respectively). The half-life of the SPECT tracer indium-111 (^{111}In) is 67.4 h. Antibodies have long half-lives of 1–3 weeks, which requires the use of radionuclides that also have long half-lives [7].

^{18}F-Fluorodeoxyglucose PET

In HNSCC patients, many PET tracers have been tested but only ^{18}F-fluorodeoxyglucose (FDG)-PET is incorporated in management guidelines. FDG-PET enables visualization and quantification of glucose metabolism which is enhanced in most tumors, but also in areas of inflammation. The National Comprehensive Cancer Network (NCCN) Clinical Practice Guidelines for head and neck cancer (version 1, 2015) recommend the use of FDG-PET/CT for patients with lymph node metastasis in the neck of a squamous cell carcinoma (SCC), adenocarcinoma, and anaplastic or undifferentiated epithelial tumors of an unknown primary site [8]. For patients with stage III and IV HNSCC, FDG-PET is considered optional because it may alter treatment decisions by upstaging patients. For response evaluation after chemoradiotherapy or radiotherapy alone, FDG-PET is recommended 12 weeks after completion of treatment in patients with a clinical response, to guide the decision on neck dissection. A meta-analysis of mainly single center small studies demonstrated a high negative predictive value of FDG-PET/CT after chemoradiotherapy for persistent/recurrent disease [9]. A recent phase III trial compared FDG-PET/CT guided active surveillance with planned neck dissection for HNSCC patients with locally advanced disease treated with primary radical chemoradiotherapy. The study showed that overall survival was equivalent. Moreover, in the surveillance arm only 20 % of the patients underwent a neck dissection, which resulted in fewer complications, better cost effectiveness, and similar quality of life [10].

Quantification of tumor FDG uptake may also have prognostic value. A meta-analysis suggested that a low tumor standardized uptake value (SUV) is associated with a better disease free survival, a better overall survival, and improved local control [11]. In a large retrospective study from Denmark, tumor FDG uptake was shown to be an independent prognostic factor in patients who received radiotherapy as primary treatment, with high tumor SUVmax corresponding to a worse failure free survival [12].

Finally, FDG-PET is under investigation as a tool to improve radiotherapy (RT) treatment planning. The observation that local recurrence after radiotherapy

frequently occurs in the area with the most intense FDG uptake has boosted trials that investigate FDG-PET based radiotherapy dose painting [13]. Two different strategies are applied: dose painting by contours, where a higher uniform RT dose is delivered to a target volume based on PET imaging; and dose painting by numbers, where on a voxel scale SUV is used to calculate RT dose.

Non-FDG PET Tracers

Apart from FDG, more than 20 PET tracers have been tested in HNSCC for imaging hypoxia, proliferation, amino acid metabolism, and other cellular processes and tumor characteristics (see Table 5.1). Especially imaging of tumor hypoxia is an area of active research.

Table 5.1 Examples of studies with non-FDG PET tracers in HNSCC patients

Tracer	First author, year	Type	Target/process
^{18}F-FMISO	Rajendran, 2006 [14]	Nitroimidazole	Hypoxia
^{18}F-FAZA	Mortensen, 2012 [15]	Nitroimidazole	Hypoxia
^{18}F-HX4	Zegers, 2015 [16]	Nitroimidazole	Hypoxia
^{18}F-EF5	Komar, 2014 [17]	Nitroimidazole	Hypoxia
^{62}Cu-ATSM	Sato, 2014 [18]	Copper semicarbazone	Hypoxia
^{64}Cu-ATSM	Grassi, 2014 [19]	Copper semicarbazone	Hypoxia
^{18}F-FLT	Hoeben, 2013 [20]	Nucleoside	Proliferation, DNA synthesis
^{11}C-4DST	Ito, 2015 [21]	Nucleoside	Proliferation, DNA synthesis
^{11}C-MET	Wedman, 2009 [22]	Amino acid	Amino acid metabolism
^{18}F-FAMT	Kim, 2015 [23]	Amino acid	Amino acid metabolism
^{18}F-FET	Pauleit, 2006 [24]	Amino acid	Amino acid metabolism
^{18}F-FMT	Burger, 2014 [25]	Amino acid	Amino acid metabolism
^{11}C-Choline	Ito, 2010 [26]	Phospholipid precursor	Phospholipid biosynthesis
^{18}F-FCH	Parashar, 2012 [27]	Phospholipid precursor	Phospholipid biosynthesis
^{15}O-H_2O	Komar, 2014 [17]	Water	Perfusion
^{68}Ga-DOTATOC	Schartinger, 2013 [28]	Octreotide	Somatostatin receptor expression
^{18}F-BPA	Tani, 2014 [29]	Boron-amino acid	Replicating cell/boron accumulation
^{18}F-5-FU	Hino-Shishikura, 2013 [30]	Cytotoxic chemotherapy	Replicating cell/drug distribution
^{89}Zr-Cetuximab	Heukelom, 2013 [31]	Antibody	EGFR expression, drug distribution
^{89}Zr-U36	Börjesson, 2009 [32]	Antibody	CD44v6 expression
^{124}I-F16SIP	Heuveling, 2013 [33]	Mini antibody	Fibronectin/angiogenesis

Hypoxia Imaging

Tumor hypoxia is associated with poor prognosis and resistance to treatment. Tumor hypoxia can be analyzed directly by measuring oxygen tension with an electrode, but this is an invasive procedure which does not take into account tumor heterogeneity. Hypoxia imaging on the other hand allows serial noninvasive assessment of tumor hypoxia, both of the primary tumor and of lymph node metastases. Multiple hypoxia PET tracers have been developed, mostly based on a nitroimidazole structure. These molecules freely diffuse through cell membranes but get trapped into cells in the presence of a low oxygen level [34, 35]. The most used hypoxia PET tracer is ^{18}F-fluoromisonidazole (^{18}F-FMISO) which has recently been reviewed by Rajendran and Krohn [36]. Several, generally small single center, ^{18}F-FMISO PET studies have been published in HNSCC patients over the last 10 years (Table 5.2). In these studies, different parameters for quantification were used, but also different reference tissues, different treatment schedules, and different timing of follow up imaging. This complicates interpretation and hampers robust conclusions. However, several studies showed that patient with more hypoxic tumors had a worse outcome [14, 37, 41, 44, 46, 50]. Furthermore, early reoxygenation during chemoradiotherapy appears to be associated with a lower risk of recurrence [46, 50].

Where prognostic markers provide information about outcome of patients independent of treatment, predictive markers give information on the effect of a specific treatment strategy [51]. The prognostic value of hypoxia PET can potentially be used to guide treatment de-escalation in patients with nonhypoxic tumors with favorable prognosis and/or treatment escalation in patients with hypoxic tumors (Fig. 5.1). Currently a treatment de-escalation study is ongoing in patients with human papillomavirus (HPV) positive oropharynx cancers that are nonhypoxic at baseline or show early re-oxygenation on repeat imaging (ClinicalTrials.gov Identifier: NCT00606294). On the other end of the spectrum, in silico studies have demonstrated the feasibility of increasing radiotherapy dose to hypoxic tumor subvolumes [53–57]. Currently two randomized studies are comparing standard chemoradiotherapy with chemoradiotherapy using an increased radiation dose to hypoxic tumor subvolumes (ClinicalTrial.gov. Identifiers: NCT02352792 and NCT01212354).

Several therapeutic strategies have been developed to reduce tumor hypoxia during radiotherapy, including carbogen and nicotinamide, tirapazamine, and nimorazol [58–60]. Hypoxia PET may have predictive value by identification of patients who benefit from hypoxia targeting treatment. This could be investigated by using a biomarker stratified study design (Fig. 5.2). Data from a sub study using ^{18}F-FMISO PET suggested that patients with hypoxic tumors derived benefit from treatment with tirapazamin, a cytotoxic drug with selective toxicity towards hypoxic cells [38]. Currently an international randomized phase III trial comparing chemoradiotherapy plus nimorazol with chemoradiotherapy plus placebo in patients with locally advanced HNSCC uses a hypoxic gene signature as stratification factor but also tests predictive value of hypoxia PET in a subset of the patients (ClinicalTrials.gov Identifier: NCT01880359). However, nimorazole

Table 5.2 ^{18}F-FMISO PET studies in HNSCC patients

Author	Year	Pt N	Treatment	Timing	Quantification parameters	Reference tissue	Prognostic value	Predictive value
Thorwarth [37]	2005	15	(C)RT	Baseline	TAC, TRP, perfusion, SUVmax, FHV	Blood	Yes	NA
Rajendran [14]	2006	73	(C)RT / surgery ± PO(C)RT	Baseline	HV, TBRmax	Blood	Yes	NA
Rischin [38]	2006	45	RT + tirapazamin vs. CRT	Baseline, week 4/5	Qualitative > background	NR	No	Yes
Eschmann [39]	2007	14	(C)RT	Baseline, 30 Gy	TAC, mean SUV, TMR	Muscle	NR	NA
Nehmeh [40]	2008	20	NR	Baseline 2×	FHV	Blood	NR	NA
Dirix [41]	2009	15	CRT	Baseline, week 4	HV, TBRmax	Blood	Yes	NA
Lee [42]	2009 [43]	20	CRT	Baseline, week 4	Qualitative > background	NR	No	NA
Kikuchi [44]	2011	17	NAC followed by surgery or (C)RT	Baseline	SUVmax, TMR	Muscle	Yes	NA
Yamane [45]	2011	14	NAC	Before + after NAC	SUVmax, TMR, HV	Muscle	NR	no
Zips [46]	2012	25	CRT	Baseline week 1, 2, 5	HV, baseline HF, SUVmax, TBRmax	Muscle	Yes	NA
Bittner [43]	2013	16	CRT	Baseline, week 2	HV	NR	NR	NA
Henriques [47]	2013	15	RT	Baseline	TBRmax, FHV 3×	NR	NR	NA
Okamoto [48]	2013	11	NR	Baseline 2×	SUVmax, TMR, TBR, HV	Muscle Blood	NR	NR

(continued)

Table 5.2 (continued)

Author	Year	Pt N	Treatment	Timing	Quantification parameters	Reference tissue	Prognostic value	Predictive value
Sato [49]	2014	22	NAC followed by surgery	Before surgery + before/ during/after NAC	SUVmax	TMR	NR	Yes
Wiedenmann [50]	2015	16	CRT	Before, week 2, 5	TBRmax, HV	Blood	Yes	NA

(*C*)*RT* (chemo)radiotherapy, *FHV* fractional hypoxic volume, *Gy* Gray, *HV* hypoxic volume, *NA* not applicable, *NAC* neoadjuvant chemotherapy, *N* number, *NR* not reported, *PO*(*C*)*RT* postoperative (chemo)radiotherapy, *Pt* patient, *SUVmax* maximum standardized uptake value, *TAC* time activity curve, *TBR* tumor-to-blood ratio, *TBRmax* maximum tumor-to-blood ratio, *TMR* tumor-to-muscle ratio, *TRP* tracer retention potential, *wk* week

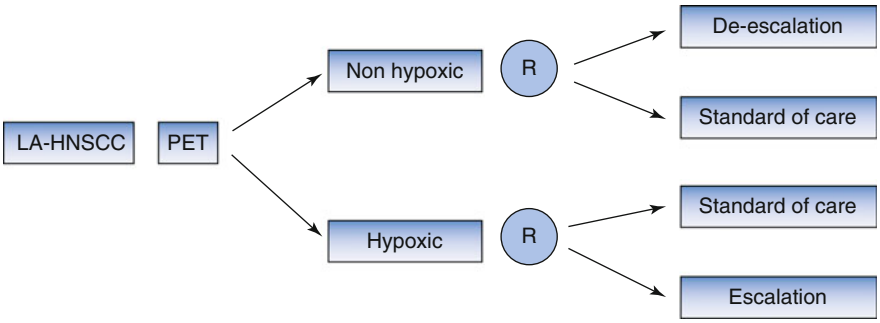

Fig. 5.1 Study design using hypoxia PET as prognostic marker. *LA-HNSCC* locally advanced head and neck squamous cell carcinoma, *PET* positron emission tomography, *R* randomization. Patients with LA-HNSCC undergo hypoxia PET imaging before start of treatment. Patients with nonhypoxic tumors are randomized between standard of care and an experimental treatment de-escalation regimen. Patients with hypoxic tumors are randomized between standard of care and an experimental treatment intensification regimen. Double enrichment design (After Freidlin et al. [52])

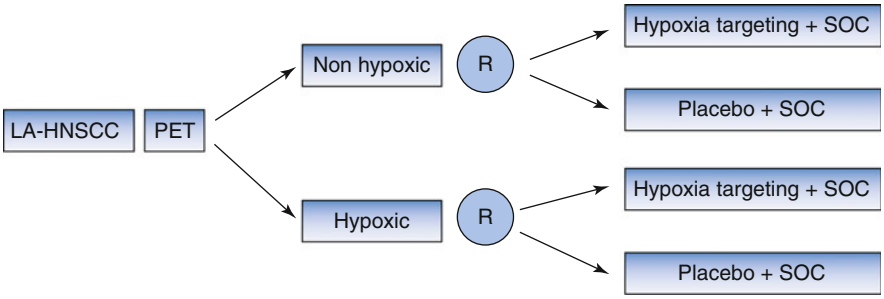

Fig. 5.2 Study design testing hypoxia PET as predictive marker. *LA-HNSCC* locally advanced head and neck squamous cell carcinoma, *PET* positron emission tomography, *R* randomization, *SOC* standard of care. Patients with LA-HNSCC undergo hypoxia PET imaging before start of treatment. Patients with nonhypoxic tumors as well as patients with hypoxic tumors are randomized between standard of care plus a hypoxia targeting drug and standard of care plus placebo. Biomarker stratified design (After Freidlin, et al. [52])

is a cheap drug with limited side effects, therefore it is doubtful if hypoxia PET is going to be implemented as predictive marker even if the positive and negative predictive values are high.

PET Imaging Using Radiolabeled Antibodies

PET imaging with radiolabeled monoclonal antibodies, also called immuno-PET, can potentially be used to select patient for targeted treatment and for drug development [5]. For HNSCC, the epidermal growth factor receptor (EGFR) blocking

antibody cetuximab is the only targeted therapy shown to be effective, in combination with radiotherapy and in combination with chemotherapy [61, 62]. EGFR, also known as human epidermal growth factor receptor 1 (HER1), is a member of the human EGFR (HER) family that further consists of HER2, HER3, and HER4.

Preclinical research has shown that activation of HER3 after dimerization with HER2 limits activity of EGFR inhibition in HNSCC and that dual inhibition of EGFR and HER3 can overcome resistance to radiation and to EGFR inhibition [63, 64]. Several agents targeting HER3 are currently under investigation in clinical trials, including monoclonal antibodies directed against HER3, dual inhibitors of EGFR and HER3, and pan-HER monoclonal antibody mixtures and tyrosine kinase inhibitors. Immuno-PET using radiolabeled antibodies against EGFR and HER3 could be useful to provide information on availability of the drug target and distribution of therapeutic antibodies in HNSCC patients.

EGFR Imaging

EGFR expression determined by immunohistochemistry has prognostic value in HNSCC, but is not a predictive biomarker for efficacy of cetuximab [65]. This may be related to heterogeneity in EGFR expression but also to accessibility of the tumor to EGFR inhibitors. Tumor drug delivery is not solely dependent on expression of the target, but also determined by perfusion, permeability, interstitial pressure, and drug characteristics including size [66, 67]. Two preclinical studies investigating ^{64}Cu-cetuximab PET imaging in xenograft models reported a correlation between tumor uptake of ^{64}Cu-cetuximab and EGFR expression [68, 69]. A third study with ^{89}Zr-cetuximab PET imaging in tumor bearing mice showed tracer uptake in EGFR positive tumors, but no correlation between tracer uptake and EGFR expression was found [70]. This may however be related to the tracer dose used [71].

Antibodies have a long half-life which implicates that in order to achieve a good tumor-to-background ratio and tumor-to-blood ratio, the optimal timing of imaging is around 7 days after tracer injection. To allow imaging within 24 h and repeat imaging early after start of treatment, antibody fragments of cetuximab (cetuximab-F(ab')$_2$) have been developed and radiolabeled for SPECT and PET imaging [72, 73]. Imaging studies in head and neck cancer xenograft models using ^{111}In-cetuximab-F(ab')$_2$ SPECT have shown that localization of the tracer correlates with EGFR expression and that the model with the highest uptake was the most sensitive to cetuximab treatment [72, 74]. Furthermore, increased tumor tracer uptake was found after radiotherapy in a cetuximab sensitive HNSCC xenograft model, which was accompanied by translocation of EGFR to the tumor cell membrane [75]. On the other hand, in a cetuximab resistant tumor model, no increase in tumor tracer uptake after radiotherapy occurred. Finally, treatment of human HNSCC xenograft models with radiotherapy alone, cetuximab alone, or the combination demonstrated reduced tracer uptake in responding tumors while in resistant tumors an increase in tumor tracer uptake was found [75]. Therefore, translation of this molecular imaging technique to

the clinic offers a promising tool for selecting patients who will benefit from treatment with cetuximab but it could also be useful as an early read-out of treatment efficacy. Three clinical studies have started using ^{89}Zr-cetuximab PET imaging, one in HNSCC and two in colorectal cancer patients (ClinicalTrials.gov Identifiers: NCT01504815, NCT02117466, NCT01691391) [31, 76]. The head and neck cancer trial was initiated as a randomized phase II study comparing cisplatin with cetuximab and standard radiotherapy with redistributed radiotherapy in a two by two factorial design. One of the objectives was to evaluate the predictive value of ^{89}Zr-cetuximab tumor uptake on a pretreatment PET scan [31]. Unfortunately the trial design has been changed and cetuximab treatment and cetuximab imaging are no longer part of the protocol (https://clinicaltrials.gov/archive/NCT01504815/2014_08_21/changes).

HER3 Imaging

The HER3 antibodies lumretuzumab and patritumab have been labeled for PET imaging [77, 78]. In a phase I study, 13 patients with solid tumors expressing HER3, determined by immunohistochemistry, underwent imaging with ^{89}Zr-lumretuzumab PET before start of treatment with the same antibody [79]. Two patients with HNSCC were included in this study. The aim of the imaging part was to determine in vivo biodistribution and the ability of the antibody to target the tumor. In all patients, tracer uptake in tumor lesions was seen. Metastases in the bone and brain that were unknown were detected in three patients. Results of serial imaging during treatment to assess HER3 saturation are awaited. In another phase I study, dosimetry of ^{64}Cu-DOTA-patritumab and receptor occupancy after a therapeutic dose patritumab were investigated [78]. Three out of six patients in the receptor occupancy cohort had a negative PET scan, likely because patients were not preselected for HER3 tumor expression. In the remaining patients, receptor occupancy was ~42 %. Larger studies are needed to assess predictive value of immuno-PET for efficacy of antibody therapy and/or for selecting the right treatment dose.

PET Imaging of Tumor Immunity

Cancer immunotherapy with immune checkpoint inhibitors has been a great breakthrough for melanoma, non–small cell lung cancer and other tumor types and has shown very promising early results in head and neck cancer [80, 81]. Antibodies directed at programmed death 1 (PD-1) and its ligand PD-L1 are currently investigated in phase III trials in HNSCC. To date there are no biomarkers that predict efficacy of immune checkpoint inhibition, although in some tumor types expression of PD-L1 using immunohistochemistry is associated with a higher response rate. Expression of relevant targets for immunotherapy may vary between and within tumor lesions, and over time. Molecular imaging offers a noninvasive platform for

serial assessment of whole body target expression and antibody distribution. PET imaging of tumor immunity is in an early phase of development with no clinical data available yet. One imaging study is currently ongoing in patients with triple negative breast cancer, bladder cancer and non–small cell lung cancer using ^{89}Zr-atezolizumab (PD-L1 antibody) PET before treatment with the same antibody (ClinicalTrials.gov Identifier: NTC02453984). Two preclinical studies already demonstrated feasibility and specificity of radiolabeled antibodies for PD-L1 imaging in tumor bearing mice [82, 83].

Another interesting strategy is to use molecular imaging as an early read-out of treatment response. PD1 and PD-L1 antibodies are supposed to act by augmenting the activity of tumor infiltrating cytotoxic T lymphocytes. Activated T lymphocytes express interleukin-2 (IL-2) receptor. SPECT imaging with radiolabeled IL-2 (^{99m}Tc- IL2) has successfully been used in patients for visualization of activated T lymphocytes in atherosclerotic plaques and in melanoma [84, 85]. For IL-2 PET imaging, which allows more sensitive and more precise quantification than SPECT, ^{18}F-IL2 has been developed and validated preclinically [86, 87].

The subset of lymphocytes that can eliminate tumor cells are CD8 expressing cytotoxic T cells. Antibody fragments against murine CD8 have successfully been labeled with ^{64}Cu and showed specific uptake in lymph nodes and spleen of antigen positive mice [88]. If this technique can successfully be translated to the clinic, it would allow to study in vivo tumor T cell infiltration which appears to be a prerequisite for immunotherapy to be effective.

Another important class of immune cells affecting tumor behavior are the tumor associated macrophages (TAMs). The subset of M2 macrophages appears to have a tumor promoting and cytotoxic T cell suppressive effect [89]. Macrophage depleting drugs are currently investigated in clinical trials. M2 macrophages specifically express the macrophage mannose receptor (MMR). Radiolabeled antibody fragments targeting MMR have been developed for PET imaging and showed specific uptake in tissues and tumors expressing MMR in mice [90]. MMR imaging could be helpful in the process of drug development, for patient selection, and as a read out for treatment efficacy.

Optical Imaging

Optical molecular imaging is a much more recent field of research, and evidence from clinical studies is still scarce. Optical imaging techniques use illumination with light of different wave lengths, ranging from safe ultraviolet range (350–400 nm), and the visible spectrum (400–750 nm) to infrared regions (750–1000 nm). Penetration of light is limited due to scattering and absorption, which vary substantially in different target tissues. Generally, in the range of 350–1000 nm, light penetration is deeper with increasing wavelength. Near-infrared (NIR) fluorescence imaging can visualize structures up to 8 mm below the surface, depending on the optical properties of the target tissue [91]. Several optical spectroscopy and imaging technologies have been and are currently investigated in HNSCC, including Raman spectroscopy, narrow band imaging, autofluorescence and exogenous fluorophore

imaging, optical coherence tomography, confocal laser endomicroscopy, and confocal reflectance microscopy [92]. Optical imaging is currently investigated for its potential to differentiate malignant lesions from normal tissue, and from benign and premalignant lesions. Optical imaging can be used during endoscopy but also intraoperatively to guide surgical resection margins. However, in cancer diagnosis, most optical techniques are either difficult to apply in vivo (i.e., Raman spectroscopy) or have not shown to yield sufficient specificity to support routine clinical use. Only in certain fields optical imaging techniques have shown to aid the clinician in diagnostic procedures. For instance, narrow band imaging helps to identify (pre)malignant lesions in head and neck cancer [93]. Here we present examples of molecular optical imaging using fluorescently labeled molecules that target specific tumor characteristics to improve the contrast between cancer and non-cancer tissue.

EGFR Imaging

In the first clinical trial on molecular optical imaging in HNSCC patients, cetuximab labeled with the NIR fluorescent dye IRDye800 was systemically injected 3–4 days before surgery in a dose finding study [94, 95]. Wide field NIR imaging was performed at day 0, day 1, and immediately before surgery, and closed field NIR imaging of fresh tissue slices of 4–5 mm was done. After histologic preparation, a corresponding slide was analyzed with a fluorescence scanning system for comparison with immunohistochemistry. Cetuximab-IRDye800 specifically accumulated in tumor lesions with a sharp demarcation of the tumor border. The mean fluorescence intensity signal was highly correlated with EGFR expression (Fig. 5.3) [94].

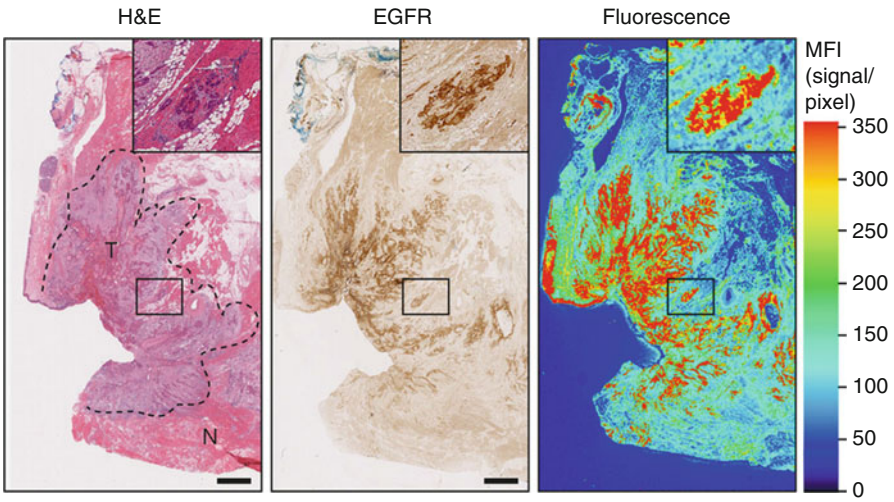

Fig. 5.3 Co-localization of fluorescence signals of cetuximab-IRDye800CW and epidermal growth factor receptor (*EGFR*) expression. Representative hemotoxylin/eosin (*H&E*) image indicating tumor (*T*) and normal (*N*) with corresponding EGFR expression immunohistochemistry stain and fluorescence image [94]

However, in tumor areas with necrosis and in areas with mature, differentiated keratinizing cancer cells, fluorescence was low despite high EGFR expression. The latter might be explained by loss of ligand binding affinity of EGFR during maturation [94]. Of interest, the highest tracer dose (62.5 mg/m^2) suggested receptor saturation according to the authors, because the tumor-to-background ratio seemed to have reached a plateau. This raises the question whether the standard therapeutic cetuximab loading dose of 400 mg/m^2 followed by weekly doses of 250 mg/m^2 might be too high, and imposes unnecessary off-target effects. However, tumor-to-background ratio may also be reduced due to a higher background fluorescence which occurs by increasing the cetuximab-IRDye800 dose. The study also revealed cetuximab-IRDye800 localization in sebaceous glands and basal cells which might be related to the skin toxicity that is frequently seen during cetuximab therapy. This novel imaging technique is an interesting tool for intraoperative use to lower the rate of involved or close surgical margins. Next to this, studying the localization of the cetuximab-IRDye800 in histological slides of the excised tumor may add another dimension to the pathology report which could be useful in determining postoperative strategies.

In a xenograft study of human oral cavity squamous cell carcinoma, fluorescent optical imaging was used to investigate whether tumor uptake of the cetuximab-IRDye800 could be improved by pretreatment with bevacizumab, a monoclonal antibody targeting human vascular endothelial growth factor A (VEGF-A) [96]. Neoadjuvant bevacizumab administration but not simultaneous bevacizumab increased cetuximab-IRDye800 tumor accumulation. This was accompanied by a higher pericyte coverage of tumor blood vessels compared to mice that did not receive bevacizumab, which suggests vascular normalization. Translating such a study design to the clinic could provide important information on effective treatment combinations and schedules.

Quantum dots (QDs) are semiconductor nanocrystals with a wide excitation and a small emission spectrum that can be conjugated to antibodies and peptides for molecular optical imaging. The size of QDs determines emission wave length, which can vary from the UV to the NIR range. A NIR QD800-EGFR antibody has been used for in vivo imaging of mice with a human orthotopic oral cavity squamous cell carcinoma [97]. Specific binding to tumor cells with a high signal-to-noise ratio up to 6 h after intravenous injection was demonstrated.

Another interesting development is topical application of a fluorescently labeled EGF peptide (EGF-Alexa 647) for early detection of oral neoplasia [98]. Immediately after excision, oral neoplastic lesions and paired normal tissue biopsies were incubated with EGF-Alexa 647 showing a consistently higher fluorescent signal in lesions which corresponded with EGFR immunohistochemistry. Clinically applicable conjugates are under development.

Integrin $\alpha_v\beta_3$ Imaging

Integrin $\alpha_v\beta_3$ is expressed by endothelial cells during angiogenesis in many cancers, including HNSCC, and by some tumor cells. Peptides containing an arginine-glycine-aspartic acid (RGD) sequence bind to $\alpha_v\beta_3$ integrin. A tetravalent RDG

peptide labeled with a NIR fluorescent molecule (AngioStamp800) is commercially available for preclinical optical imaging. Using this probe in an $\alpha_v\beta_3$ expressing orthotopic HNSCC xenograft model, Atallah et al. operated 12 mice with the use of integrin $\alpha_v\beta_3$ imaging and 12 mice with visual guidance only [99]. In the first group, after visual complete resection, tumor beds contained fluorescent spots in all mice, and 35 out of 37 specimens of these fluorescent spots contained tumor foci. Furthermore, recurrence free survival after 2 months was 75 % in mice that had $\alpha_v\beta_3$ integrin imaging guided surgery compared to 25 % in mice resected without optical imaging. In a second study by the same group, mice were followed for lymph node recurrence after resection of orthotopic HNSCC [100]. Intraoperative integrin $\alpha_v\beta_3$ imaging correctly identified clinical and subclinical lymph node metastases in these mice.

Quantum dots conjugated with RGD (QD800-RGD) have also been used for integrin $\alpha_v\beta_3$ imaging in mice bearing HNSCC. The xenografted human oral squamous cell carcinoma cell line did not express integrin $\alpha_v\beta_3$ but specific targeting of tumor vessels in this mouse model resulted in clear tumor fluorescence with the highest tumor-to-background ratio 6 h after intravenous injection of QD800-RGD [101].

Other Optical Imaging Targets

Cancer cells display aberrant glycosylation of cell surface proteins and lipids with increased sialic acid content. This has been exploited for optical imaging using topical application of wheat germ agglutinin (WGA) conjugated with fluorophores in the UV range (Alexa Fluor 350) and NIR range (Alexa Fluor 647)[102]. Ex vivo imaging of tumor and normal mucosa biopsies of patients with HNSCC demonstrated a satisfactory signal-to-noise ratio.

Another characteristic of many cancers is overexpression of cyclooxygenase-2 (COX-2). Fluorocoxib, a COX-2 targeted NIR probe, has been developed for optical imaging [103]. Specific uptake in COX-2 overexpressing human HNSCC xenografts was demonstrated with an optimal signal-to-noise ratio at 7 days post injection in mice.

Interestingly, also a NIR dye conjugated PD-L1 antibody was successfully tested in tumor bearing mice [83].

Finally, also tumor M2 macrophage recruitment has been visualized with optical imaging using an antibody against MMR (αCD206) conjugated with NIR dyes in a murine breast cancer model [104, 105].

Future Perspectives

Molecular imaging with radiolabeled ligands for PET imaging provides whole body information on distribution of targets and/or drugs with low resolution. Optical imaging gives local information with very high resolution but with limited

penetration. These complementary techniques can be used simultaneously by injecting molecules labeled with a fluorescent dye and a radionuclide [106].

Furthermore, for optical imaging, several tumor characteristics have already been analyzed simultaneously by using probes with different excitation wavelengths in preclinical studies [107].

Molecular imaging cannot replace anatomical imaging or biopsies but can potentially provide additional information to improve diagnosis and treatment of HNSCC. Before implementation, large well powered clinical studies are needed to assess its added value. Alternatively, data from multiple small studies can be combined which could be facilitated by creating ware houses with imaging data. The currently publicly available databases for genomics could serve as a role model in this respect. However, standardization of techniques and endpoints is critical for combined analysis.

References

1. Mankoff DA. A definition of molecular imaging. J Nucl Med. 2007;48:18N, 21N.
2. Chou SW, Shau YH, Wu PC, Yang YS, Shieh DB, Chen CC. In vitro and in vivo studies of FePt nanoparticles for dual modal CT/MRI molecular imaging. J Am Chem Soc. 2010;132:13270–8.
3. Shi Y, Oeh J, Eastham-Anderson J, Yee S, Finkle D, Peale Jr FV, et al. Mapping in vivo tumor oxygenation within viable tumor by ^{19}F-MRI and multispectral analysis. Neoplasia. 2013;15:1241–50.
4. Paefgen V, Doleschel D, Kiessling F. Evolution of contrast agents for ultrasound imaging and ultrasound-mediated drug delivery. Front Pharmacol. 2015;6:197.
5. Lamberts LE, Williams SP, Terwisscha van Scheltinga AG, Lub-de Hooge MN, Schröder CP, Gietema JA, et al. Antibody positron emission tomography imaging in anticancer drug development. J Clin Oncol. 2015;33:1491–504.
6. Cammaroto G, Quartuccio N, Sindoni A, Di Mauro F, Caobelli F, Young AIMN Working Group. The role of PET/CT in the management of patients affected by head and neck tumors: a review of the literature. Eur Arch Otorhinolaryngol. 2016;273(8):1961–73.
7. Knowles SM, Wu AM. Advances in immuno-positron emission tomography: antibodies for molecular imaging in oncology. J Clin Oncol. 2012;30:3884–92.
8. NCCN Guidelines version 1. 2015. www.nccn.org/professionals/physician_gls/pdf/head-and-neck.pdf. Accessed 19 Dec 2015.
9. Isles MG, McConkey C, Mehanna HM. A systematic review and meta-analysis of the role of positron emission tomography in the follow up of head and neck squamous cell carcinoma following radiotherapy or chemoradiotherapy. Clin Otolaryngol. 2008;33:210–22.
10. Mehanna H, Wong WL, McConkey CC, Rahman JK, Robinson M, Hartley AG, et al. PET-CT surveillance versus neck dissection in advanced head and neck cancer. N Engl J Med. 2016;374:1444–54.
11. Xie P, Li M, Zhao H, Sun X, Fu Z, Yu J. 18F-FDG PET or PET-CT to evaluate prognosis for head and neck cancer: a meta-analysis. J Cancer Res Clin Oncol. 2011;137:1085–93.
12. Rasmussen JH, Vogelius IR, Fischer BM, Friborg J, Aznar MC, Persson GF, et al. Prognostic value of ^{18}F-fludeoxyglucose uptake in 287 patients with head and neck squamous cell carcinoma. Head Neck. 2015;37:1274–81.
13. Differding S, Hanin FX, Grégoire V. PET imaging biomarkers in head and neck cancer. Eur J Nucl Med Mol Imaging. 2015;42:613–22.

14. Rajendran JG, Schwartz DL, O'Sullivan J, Peterson LM, Ng P, Scharnhorst J, et al. Tumor hypoxia imaging with [F-18] fluoromisonidazole positron emission tomography in head and neck cancer. Clin Cancer Res. 2006;12:5435–41.
15. Mortensen LS, Johansen J, Kallehauge J, Primdahl H, Busk M, Lassen P, et al. FAZA PET/CT hypoxia imaging in patients with squamous cell carcinoma of the head and neck treated with radiotherapy: results from the DAHANCA 24 trial. Radiother Oncol. 2012;105:14–20.
16. Zegers CM, van Elmpt W, Hoebers FJ, Troost EG, Öllers MC, Mottaghy FM, et al. Imaging of tumour hypoxia and metabolism in patients with head and neck squamous cell carcinoma. Acta Oncol. 2015;54:1378–84.
17. Komar G, Lehtiö K, Seppänen M, Eskola O, Levola H, Lindholm P, et al. Prognostic value of tumour blood flow, [^{18}F]EF5 and [^{18}F]FDG PET/CT imaging in patients with head and neck cancer treated with radiochemotherapy. Eur J Nucl Med Mol Imaging. 2014;41:2042–50.
18. Sato Y, Tsujikawa T, Oh M, Mori T, Kiyono Y, Fujieda S, et al. Assessing tumor hypoxia in head and neck cancer by PET with ^{62}Cu-diacetyl-bis(N^4-methylthiosemicarbazone). Clin Nucl Med. 2014;39:1027–32.
19. Grassi I, Nanni C, Cicoria G, Blasi C, Bunkheila F, Lopci E, et al. Usefulness of ^{64}Cu-ATSM in head and neck cancer: a preliminary prospective Study. Clin Nucl Med. 2014;39:e59–63.
20. Hoeben BA, Troost EG, Span PN, van Herpen CM, Bussink J, Oyen WJ, et al. ^{18}F-FLT PET during radiotherapy or chemoradiotherapy in head and neck squamous cell carcinoma is an early predictor of outcome. J Nucl Med. 2013;54:532–40.
21. Ito K, Yokoyama J, Miyata Y, Toyohara J, Okasaki M, Minamimoto R, et al. Volumetric comparison of positron emission tomography/computed tomography using 4′-[methyl-^{11}C]-thiothymidine with 2-deoxy-2-^{18}F-fluoro-D-glucose in patients with advanced head and neck squamous cell carcinoma. Nucl Med Commun. 2015;36:219–25.
22. Wedman J, Pruim J, Langendijk JA, van der Laan BF. Visualization of small glottic laryngeal cancer using methyl-labeled ^{11}C-methionine positron emission tomography. Oral Oncol. 2009;45:703–5.
23. Kim M, Achmad A, Higuchi T, Arisaka Y, Yokoo H, Yokoo S, et al. Effects of intratumoral inflammatory process on ^{18}F-FDG uptake: pathologic and comparative study with ^{18}F-fluoro-α-methyltyrosine PET/CT in oral squamous cell carcinoma. J Nucl Med. 2015;56:16–21.
24. Pauleit D, Zimmermann A, Stoffels G, Bauer D, Risse J, Flüss MO, et al. 18F-FET PET compared with ^{18}F-FDG PET and CT in patients with head and neck cancer. J Nucl Med. 2006;47:256–61.
25. Burger IA, Zitzmann-Kolbe S, Pruim J, Friebe M, Graham K, Stephens A, et al. First clinical results of (D)-^{18}F-Fluoromethyltyrosine (BAY 86–9596) PET/CT in patients with non-small cell lung cancer and head and neck squamous cell carcinoma. J Nucl Med. 2014;55:1778–85.
26. Ito K, Yokoyama J, Kubota K, Morooka M, Shiibashi M, Matsuda H. ^{18}F-FDG versus ^{11}C-choline PET/CT for the imaging of advanced head and neck cancer after combined intra-arterial chemotherapy and radiotherapy: the time period during which PET/CT can reliably detect non-recurrence. Eur J Nucl Med Mol Imaging. 2010;37:1318–27.
27. Parashar B, Wernicke AG, Rice S, Osborne J, Singh P, Nori D, et al. Early assessment of radiation response using a novel functional imaging modality -[^{18}F]fluorocholine PET (FCH-PET): a pilot study. Discov Med. 2012;14:13–20.
28. Schartinger VH, Dudás J, Decristoforo C, Url C, Schnabl J, Göbel G, et al. ^{68}Ga-DOTA^0-Tyr^3-octreotide positron emission tomography in head and neck squamous cell carcinoma. Med Mol Imaging. 2013;40:1365–72.
29. Tani H, Kurihara H, Hiroi K, Honda N, Yoshimoto M, Kono Y, et al. Correlation of ^{18}F-BPA and ^{18}F-FDG uptake in head and neck cancers. Radiother Oncol. 2014;113:193–7.
30. Hino-Shishikura A, Suzuki A, Minamimoto R, Shizukuishi K, Oka T, Tateishi U, et al. Biodistribution and radiation dosimetry of [^{18}F]-5-fluorouracil. Appl Radiat Isot. 2013;75:11–7.
31. Heukelom J, Hamming O, Bartelink H, Hoebers F, Giralt J, Herlestam T, et al. Adaptive and innovative radiation treatment FOR improving cancer treatment outcomE (ARTFORCE); a

randomized controlled phase II trial for individualized treatment of head and neck cancer. BMC Cancer. 2013;13:84.
32. Börjesson PK, Jauw YW, de Bree R, Roos JC, Castelijns JA, Leemans CR, et al. Radiation dosimetry of ^{89}Zr-labeled chimeric monoclonal antibody U36 as used for immuno-PET in head and neck cancer patients. J Nucl Med. 2009;50:1828–36.
33. Heuveling DA, de Bree R, Vugts DJ, Huisman MC, Giovannoni L, Hoekstra OS, et al. Phase 0 microdosing PET study using the human mini antibody F16SIP in head and neck cancer patients. J Nucl Med. 2013;54:397–401.
34. Lopci E, Grassi I, Chiti A, Nanni C, Cicoria G, Toschi L, et al. PET radiopharmaceuticals for imaging of tumor hypoxia: a review of the evidence. Am J Nucl Med Mol Imaging. 2014;4:365–84.
35. Peeters SG, Zegers CM, Yaromina A, Van Elmpt W, Dubois L, Lambin P. Current preclinical and clinical applications of hypoxia PET imaging using 2-nitroimidazoles. Q J Nucl Med Mol Imaging. 2015;59:39–57.
36. Rajendran JG, Krohn KA. F-18 fluoromisonidazole for imaging tumor hypoxia: imaging the microenvironment for personalized cancer therapy. Semin Nucl Med. 2015;45:151–62.
37. Thorwarth D, Eschmann SM, Scheiderbauer J, Paulsen F, Alber M. Kinetic analysis of dynamic ^{18}F-fluoromisonidazole PET correlates with radiation treatment outcome in head-and-neck cancer. BMC Cancer. 2005;5:152.
38. Rischin D, Hicks RJ, Fisher R, Binns D, Corry J, Porceddu S, et al. Prognostic significance of [^{18}F]-misonidazole positron emission tomography-detected tumor hypoxia in patients with advanced head and neck cancer randomly assigned to chemoradiation with or without tirapazamine: a substudy of Trans-Tasman Radiation Oncology Group Study 98.02. J Clin Oncol. 2006;24:2098–104.
39. Eschmann SM, Paulsen F, Bedeshem C, Machulla HJ, Hehr T, Bamberg M, et al. Hypoxia-imaging with ^{18}F-Misonidazole and PET: changes of kinetics during radiotherapy of head-and-neck cancer. Radiother Oncol. 2007;83:406–10.
40. Nehmeh SA, Lee NY, Schröder H, Squire O, Zanzonico PB, Erdi YE, et al. Reproducibility of intratumor distribution of ^{18}F-fluoromisonidazole in head and neck cancer. Int J Radiat Oncol Biol Phys. 2008;70:235–42.
41. Dirix P, Vandecaveye V, De Keyzer F, Stroobants S, Hermans R, Nuyts S. Dose painting in radiotherapy for head and neck squamous cell carcinoma: value of repeated functional imaging with ^{18}F-FDG PET, ^{18}F-fluoromisonidazole PET, diffusion-weighted MRI, and dynamic contrast-enhanced MRI. J Nucl Med. 2009;50:1020–7.
42. Lee N, Nehmeh S, Schöder H, Fury M, Chan K, Ling CC, et al. Prospective trial incorporating pre-/mid-treatment [^{18}F]-misonidazole positron emission tomography for head-and-neck cancer patients undergoing concurrent chemoradiotherapy. Int J Radiat Oncol Biol Phys. 2009;75:101–8.
43. Bittner MI, Wiedenmann N, Bucher S, Hentschel M, Mix M, Weber WA, et al. Exploratory geographical analysis of hypoxic subvolumes using ^{18}F-MISO-PET imaging in patients with head and neck cancer in the course of primary chemoradiotherapy. Radiother Oncol. 2013;108:511–6.
44. Kikuchi M, Yamane T, Shinohara S, Fujiwara K, Hori SY, Tona Y, et al. 18F-fluoromisonidazole positron emission tomography before treatment is a predictor of radiotherapy outcome and survival prognosis in patients with head and neck squamous cell carcinoma. Ann Nucl Med. 2011;25:625–33.
45. Yamane T, Kikuchi M, Shinohara S, Senda M. Reduction of [^{18}F]fluoromisonidazole uptake after neoadjuvant chemotherapy for head and neck squamous cell carcinoma. Mol Imaging Biol. 2011;13:227–31.
46. Zips D, Zöphel K, Abolmaali N, Perrin R, Abramyuk A, Haase R, et al. Exploratory prospective trial of hypoxia-specific PET imaging during radiochemotherapy in patients with locally advanced head-and-neck cancer. Radiother Oncol. 2012;105:21–8.
47. Henriques de Figueiredo B, Merlin T, de Clermont-Gallerande H, Hatt M, Vimont D, Fernandez P, et al. Potential of [18F]-fluoromisonidazole positron-emission tomography for

radiotherapy planning in head and neck squamous cell carcinomas. Strahlenther Onkol. 2013;189:1015–9.
48. Okamoto S, Shiga T, Yasuda K, Ito YM, Magota K, Kasai K, et al. High reproducibility of tumor hypoxia evaluated by ^{18}F-fluoromisonidazole PET for head and neck cancer. J Nucl Med. 2013;54:201–7.
49. Sato J, Kitagawa Y, Yamazaki Y, Hata H, Asaka T, Miyakoshi M, et al. Advantage of FMISO-PET over FDG-PET for predicting histological response to preoperative chemotherapy in patients with oral squamous cell carcinoma. Eur J Nucl Med Mol Imaging. 2014;41:2031–41.
50. Wiedenmann NE, Bucher S, Hentschel M, Mix M, Vach W, Bittner MI, et al. Serial [18F]-fluoromisonidazole PET during radiochemotherapy for locally advanced head and neck cancer and its correlation with outcome. Radiother Oncol. 2015;117:113–7.
51. Oldenhuis CN, Oosting SF, Gietema JA, de Vries EG. Prognostic versus predictive value of biomarkers in oncology. Eur J Cancer. 2008;44:946–53.
52. Freidlin B, McShane LM, Korn EL. Randomized clinical trials with biomarkers: design issues. J Natl Cancer Inst. 2010;102:152–60.
53. Lin Z, Mechalakos J, Nehmeh S, Schoder H, Lee N, Humm J, et al. The influence of changes in tumor hypoxia on dose-painting treatment plans based on ^{18}F-FMISO positron emission tomography. Int J Radiat Oncol Biol Phys. 2008;70:1219–28.
54. Lee NY, Mechalakos JG, Nehmeh S, Lin Z, Squire OD, Cai S, et al. Fluorine-18-labeled fluoromisonidazole positron emission and computed tomography-guided intensity-modulated radiotherapy for head and neck cancer: a feasibility study. Int J Radiat Oncol Biol Phys. 2008;70:2–13.
55. Choi W, Lee SW, Park SH, Ryu JS, Oh SJ, Im KC, et al. Planning study for available dose of hypoxic tumor volume using fluorine-18-labeled fluoromisonidazole positron emission tomography for treatment of the head and neck cancer. Radiother Oncol. 2010;97:176–82.
56. Toma-Dasu I, Uhrdin J, Antonovic L, Dasu A, Nuyts S, Dirix P, et al. Dose prescription and treatment planning based on FMISO-PET hypoxia. Acta Oncol. 2012;51:222–30.
57. Henriques de Figueiredo B, Zacharatou C, Galland-Girodet S, Benech J, De Clermont-Gallerande H, Lamare F, et al. Hypoxia imaging with [18F]-FMISO-PET for guided dose escalation with intensity-modulated radiotherapy in head-and-neck cancers. Strahlenther Onkol. 2015;191:217–24.
58. Janssens GO, Rademakers SE, Terhaard CH, Doornaert PA, Bijl HP, van den Ende P, et al. Accelerated radiotherapy with carbogen and nicotinamide for laryngeal cancer: results of a phase III randomized trial. J Clin Oncol. 2012;30:1777–83.
59. Rischin D, Peters LJ, O'Sullivan B, Giralt J, Fisher R, Yuen K, et al. Tirapazamine, cisplatin, and radiation versus cisplatin and radiation for advanced squamous cell carcinoma of the head and neck (TROG 02.02, HeadSTART): a phase III trial of the Trans-Tasman Radiation Oncology Group. J Clin Oncol. 2010;28:2989–95.
60. Overgaard J, Hansen HS, Overgaard M, Bastholt L, Berthelsen A, Specht L, et al. A randomized double-blind phase III study of nimorazole as a hypoxic radiosensitizer of primary radiotherapy in supraglottic larynx and pharynx carcinoma. Results of the Danish Head and Neck Cancer Study (DAHANCA) Protocol 5–85. Radiother Oncol. 1998;46:135–46.
61. Bonner JA, Harari PM, Giralt J, Azarnia N, Shin DM, Cohen RB, et al. Radiotherapy plus cetuximab for squamous-cell carcinoma of the head and neck. N Engl J Med. 2006;354:567–78.
62. Vermorken JB, Mesia R, Rivera F, Remenar E, Kawecki A, Rottey S, et al. Platinum-based chemotherapy plus cetuximab in head and neck cancer. N Engl J Med. 2008;359:1116–27.
63. Zhang L, Castanaro C, Luan B, Yang K, Fan L, Fairhurst JL, et al. ERBB3/HER2 signaling promotes resistance to EGFR blockade in head and neck and colorectal cancer models. Mol Cancer Ther. 2014;13:1345–55.
64. Huang S, Li C, Armstrong EA, Peet CR, Saker J, Amler LC, et al. Dual targeting of EGFR and HER3 with MEHD7945A overcomes acquired resistance to EGFR inhibitors and radiation. Cancer Res. 2013;73:824–33.
65. Licitra L, Störkel S, Kerr KM, Van Cutsem E, Pirker R, Hirsch FR, et al. Predictive value of epidermal growth factor receptor expression for first-line chemotherapy plus cetuximab in

patients with head and neck and colorectal cancer: analysis of data from the EXTREME and CRYSTAL studies. Eur J Cancer. 2013;49:1161–8.
66. Chauhan VP, Stylianopoulos T, Martin JD, Popović Z, Chen O, Kamoun WS, et al. Normalization of tumour blood vessels improves the delivery of nanomedicines in a size-dependent manner. Nat Nanotechnol. 2012;7:383–8.
67. Arjaans M, Schröder CP, Oosting SF, Dafni U, Kleibeuker JE, de Vries EG. VEGF pathway targeting agents, vessel normalization and tumor drug uptake: from bench to bedside. Oncotarget. 2016. doi:10.18632/oncotarget.6918. [Epub ahead of print].
68. Cai W, Chen K, He L, Cao Q, Koong A, Chen X. Quantitative PET of EGFR expression in xenograft-bearing mice using 64Cu-labeled cetuximab, a chimeric anti-EGFR monoclonal antibody. Eur J Nucl Med Mol Imaging. 2007;34:850–8.
69. Ping Li W, Meyer LA, Capretto DA, Sherman CD, Anderson CJ. Receptor-binding, biodistribution, and metabolism studies of 64Cu-DOTA-cetuximab, a PET-imaging agent for epidermal growth-factor receptor-positive tumors. Cancer Biother Radiopharm. 2008; 23:158–71.
70. Aerts HJ, Dubois L, Perk L, Vermaelen P, van Dongen GA, Wouters BG, et al. Disparity between in vivo EGFR expression and ^{89}Zr-labeled cetuximab uptake assessed with PET. J Nucl Med. 2009;50:123–31.
71. van Dijk LK, Boerman OC, Kaanders JH, Bussink J. PET imaging in head and neck cancer patients to monitor treatment response: a future role for EGFR-targeted imaging. Clin Cancer Res. 2015;21:3602–9.
72. van Dijk LK, Hoeben BA, Stegeman H, Kaanders JH, Franssen GM, Boerman OC, et al. ^{111}In-cetuximab-F(ab')2 SPECT imaging for quantification of accessible epidermal growth factor receptors (EGFR) in HNSCC xenografts. Radiother Oncol. 2013;108:484–8.
73. van Dijk LK, Yim CB, Franssen GM, Kaanders JH, Rajander J, Solin O, et al. PET of EGFR with (64) Cu-cetuximab-F(ab')2 in mice with head and neck squamous cell carcinoma xenografts. Contrast Media Mol Imaging. 2016;11:65–70.
74. van Dijk LK, Boerman OC, Franssen GM, Lok J, Kaanders JH, Bussink J. Early response monitoring with ^{18}F-FDG PET and cetuximab-F(ab')2-SPECT after radiotherapy of human head and neck squamous cell carcinomas in a mouse model. J Nucl Med. 2014;55:1665–70.
75. van Dijk LK, Boerman OC, Franssen GM, Kaanders JH, Bussink J. ^{111}In-cetuximab-F(ab')2 SPECT and ^{18}F-FDG PET for prediction and response monitoring of combined-modality treatment of human head and neck carcinomas in a mouse model. J Nucl Med. 2015;56:287–92.
76. Makris NE, Boellaard R, van Lingen A, Lammertsma AA, van Dongen GA, Verheul HM, et al. PET/CT-derived whole-body and bone marrow dosimetry of ^{89}Zr-cetuximab. J Nucl Med. 2015;56:249–54.
77. Terwisscha van Scheltinga AG, Lub-de Hooge MN, Abiraj K, Schröder CP, Pot L, Bossenmaier B, et al. ImmunoPET and biodistribution with human epidermal growth factor receptor 3 targeting antibody ^{89}Zr-RG7116. MAbs. 2014;6:1051–8.
78. Lockhart AC, Liu Y, Dehdashti F, Laforest R, Picus J, Frye J, et al. Phase 1 evaluation of [^{64}Cu]DOTA-patritumab to assess dosimetry, apparent receptor occupancy, and safety in subjects with advanced solid tumors. Mol Imaging Biol. 2015;18(3):446–53.
79. Bensch F, Lamberts, LE, Lub-de Hooge MN, Terwisscha van Scheltinga AG, de Jong JR, Gietema JA, et al. Phase I imaging study of the HER3 antibody RG7116 using ^{89}Zr-RG7116 PET in patients with metastatic or locally advanced HER 3 positive solid tumors. J Clin Oncol. 2014;32 Suppl 15. abstract 11095.
80. Segal NH, Ou SI, Balmanoukian AS, Fury MG, Massarelli E, Brahmer JR, et al. Safety and efficacy of MEDI4736, an anti-PD-L1 antibody, in patients from a squamous cell carcinoma of the head and neck (SCCHN) expansion cohort. J Clin Oncol. 2015;33 Suppl 15. abstract 3011.
81. Chow LQ, Haddad R, Gupta S, Mahipal A, Mehra R, Tahara M, et al. Antitumor activity of pembrolizumab in biomarker-unselected patients with recurrent and/or metastatic head and neck squamous cell carcinoma: results from the KEYNOTE-012 expansion cohort. J Clin Oncol. 2016; Sep 19. pii: JCO681478. [Epub ahead of print]

82. Heskamp S, Hobo W, Molkenboer-Kuenen JD, Olive D, Oyen WJ, Dolstra H, et al. Noninvasive imaging of tumor PD-L1 expression using radiolabeled anti-PD-L1 antibodies. Cancer Res. 2015;75:2928–36.
83. Chatterjee S, Lesniak WG, Gabrielson M, Lisok A, Wharram B, Sysa-Shah P, et al. A humanized antibody for imaging immune checkpoint ligand PD-L1 expression in tumors. Oncotarget. 2016;7(9):10215–27. doi:10.18632/oncotarget.7143. [Epub ahead of print].
84. Glaudemans AW, Bonanno E, Galli F, Zeebregts CJ, de Vries EF, Koole M, et al. In vivo and in vitro evidence that ^{99}mTc-HYNIC-interleukin-2 is able to detect T lymphocytes in vulnerable atherosclerotic plaques of the carotid artery. Eur J Nucl Med Mol Imaging. 2014;41:1710–9.
85. Signore A, Annovazzi A, Barone R, Bonanno E, D'Alessandria C, Chianelli M, et al. ^{99m}Tc-interleukin-2 scintigraphy as a potential tool for evaluating tumor-infiltrating lymphocytes in melanoma lesions: a validation study. J Nucl Med. 2004;45:1647–52.
86. Di Gialleonardo V, Signore A, Willemsen AT, Sijbesma JW, Dierckx RA, de Vries EF. Pharmacokinetic modelling of *N*-(4-[^{18}F]fluorobenzoyl)interleukin-2 binding to activated lymphocytes in an xenograft model of inflammation. Eur J Nucl Med Mol Imaging. 2012;39:1551–60.
87. Di Gialleonardo V, Signore A, Glaudemans AW, Dierckx RA, De Vries EF. *N*-(4-^{18}F-fluorobenzoyl)interleukin-2 for PET of human-activated T lymphocytes. J Nucl Med. 2012;53:679–86.
88. Tavaré R, McCracken MN, Zettlitz KA, Knowles SM, Salazar FB, Olafsen T, et al. Engineered antibody fragments for immuno-PET imaging of endogenous CD8+ T cells in vivo. Proc Natl Acad Sci U S A. 2014;111:1108–13.
89. Komohara Y, Fujiwara Y, Ohnishi K, Takeya M. Tumor-associated macrophages: potential therapeutic targets for anti-cancer therapy. Adv Drug Deliv Rev. 2015. doi:10.1016/j.addr.2015.11.009. [Epub ahead of print] Review.
90. Blykers A, Schoonooghe S, Xavier C, D'hoe K, Laoui D, D'Huyvetter M, et al. PET Imaging of macrophage mannose receptor-expressing macrophages in tumor stroma using ^{18}F-radiolabeled camelid single-domain antibody fragments. J Nucl Med. 2015;56:1265–71.
91. Vahrmeijer AL, Hutteman M, van der Vorst JR, van de Velde CJ, Frangioni JV. Image-guided cancer surgery using near-infrared fluorescence. Nat Rev Clin Oncol. 2013;10:507–18.
92. Davies K, Connolly JM, Dockery P, Wheatley AM, Olivo M, Keogh I. Point of care optical diagnostic technologies for the detection of oral and oropharyngeal squamous cell carcinoma. Surgeon. 2015;13:321–9.
93. Muto M, Minashi K, Yano T, Saito Y, Oda I, Nonaka S, et al. Early detection of superficial squamous cell carcinoma in the head and neck region and esophagus by narrow band imaging: a multicenter randomized controlled trial. J Clin Oncol. 2010;28:1566–72.
94. de Boer E, Warram JM, Tucker MD, Hartman YE, Moore LS, de Jong JS, et al. In vivo fluorescence immunohistochemistry: localization of fluorescently labeled cetuximab in squamous cell carcinomas. Sci Rep. 2015;5:10169.
95. Rosenthal EL, Warram JM, de Boer E, Chung TK, Korb ML, Brandwein-Gensler M, et al. Safety and tumor specificity of cetuximab-IRDye800 for surgical navigation in head and neck cancer. Clin Cancer Res. 2015;21:3658–66.
96. Chung TK, Warram J, Day KE, Hartman Y, Rosenthal EL. Time-dependent pretreatment with bevacuzimab increases tumor specific uptake of cetuximab in preclinical oral cavity cancer studies. Cancer Biol Ther. 2015;16:790–8.
97. Yang K, Zhang FJ, Tang H, Zhao C, Cao YA, Lv XQ, et al. In-vivo imaging of oral squamous cell carcinoma by EGFR monoclonal antibody conjugated near-infrared quantum dots in mice. Int J Nanomedicine. 2011;6:1739–45.
98. Nitin N, Rosbach KJ, El-Naggar A, Williams M, Gillenwater A, Richards-Kortum RR. Optical molecular imaging of epidermal growth factor receptor expression to improve detection of oral neoplasia. Neoplasia. 2009;11:542–51.
99. Atallah I, Milet C, Henry M, Josserand V, Reyt E, Coll JL, et al. Near-infrared fluorescence imaging-guided surgery improves recurrence-free survival rate in novel orthotopic animal

model of head and neck squamous cell carcinoma. Head Neck. 2014. doi:10.1002/hed.23980. [Epub ahead of print].
100. Atallah I, Milet C, Quatre R, Henry M, Reyt E, Coll JL, et al. Role of near-infrared fluorescence imaging in the resection of metastatic lymph nodes in an optimized orthotopic animal model of HNSCC. Eur Ann Otorhinolaryngol Head Neck Dis. 2015;132:337–42.
101. Huang H, Bai YL, Yang K, Tang H, Wang YW. Optical imaging of head and neck squamous cell carcinoma in vivo using arginine-glycine-aspartic acid peptide conjugated near-infrared quantum dots. Onco Targets Ther. 2013;6:1779–87.
102. Baeten J, Suresh A, Johnson A, Patel K, Kuriakose M, Flynn A, et al. Molecular imaging of oral premalignant and malignant lesions using fluorescently labeled lectins. Transl Oncol. 2014;7:213–20.
103. Uddin MJ, Crews BC, Ghebreselasie K, Daniel CK, Kingsley PJ, Xu S, et al. Targeted imaging of cancer by fluorocoxib C, a near-infrared cyclooxygenase-2 probe. J Biomed Opt. 2015;20:50502.
104. Sun X, Gao D, Gao L, Zhang C, Yu X, Jia B, et al. Molecular imaging of tumor-infiltrating macrophages in a preclinical mouse model of breast cancer. Theranostics. 2015;5:597–608.
105. Zhang C, Gao L, Cai Y, Liu H, Gao D, Lai J, et al. Inhibition of tumor growth and metastasis by photoimmunotherapy targeting tumor-associated macrophage in a sorafenib-resistant tumor model. Biomaterials. 2016;84:1–12.
106. Sampath L, Kwon S, Ke S, Wang W, Schiff R, Mawad ME, et al. Dual-labeled trastuzumab-based imaging agent for the detection of human epidermal growth factor receptor 2 overexpression in breast cancer. J Nucl Med. 2007;48:1501–10.
107. Mukherjee A, Shim Y, Myong SJ. Quantum dot as probe for disease diagnosis and monitoring. Biotechnol J. 2016;11:31–42.